J. Meas. Sci. Instrum., 2025, 16(4): 526-536.
DOI: 10.62756/jmsi.1674-8042.2025051
http://jmsi.publish.founderss.cn
jmsi@nuc.edu.cn

A dual-constrained watershed algorithm for bean particle segmentation and sizing

ZHUANG Licheng, GE Boang, HU Jun, SONG Yiheng, LIU Sheng*
School of Artificial Intelligence, Huaibei Normal University, Huaibei 235000, China

***Corresponding author:** LIU Sheng (Liusheng@chnu.edu.cn)

Received: September 10, 2025 **Revised:** October 22, 2025 **Accepted:** November 5, 2025

Abstract: Accurate measurement of bean particle size is essential for automated grading and quality control in agricultural processing. However, existing image segmentation methods often suffer from low efficiency, over-segmentation, and high computational cost. We proposed a distance-gradient dual constrained watershed algorithm for precise segmentation and measurement of bean particles. The method integrated distance transform-based seed extraction with gradient-constrained flooding, effectively suppressing noise-induced region fragmentation and improving the separation of adherent particles. An experimental platform was constructed using an industrial camera and an image-processing pipeline to evaluate performance. Compared with the conventional watershed algorithm, the proposed method improves segmentation accuracy by 7.2% and reduces the mean particle size error by 27.8% (0.13 mm, representing a relative error of 2.4%). Validation on three soybean varieties confirmed the robustness and generalizability of the approach. The results indicated that the proposed algorithm provided an efficient and accurate technique for agricultural particle size analysis, offering potential for integration into practical low-cost inspection systems.

Key words: distance-gradient dual constraint watershed algorithm; machine vision inspection system; particle size sorting; precision agriculture; metrology

0 Introduction

Accurate particle size measurement is essential for both industrial and agricultural applications, serving as a key indicator in quality control and process optimization[1]. In legume processing, inconsistent grain sizes can lead to higher energy consumption, reduced operational efficiency, and lower product quality[2]. Traditional methods, such as manual sieving and threshold-based image processing, suffer from low efficiency, operator dependency, and limited adaptability under dynamic conditions[3].

Recent advances in machine vision and image processing have facilitated the development of non-contact and automated sizing systems[4]. Among these, the watershed algorithm is widely applied due to its strong boundary detection capabilities[5]. However, it remains prone to over-segmentation and demands careful initialization[6]. Wang et al.[7] improved segmentation accuracy by enhancing the watershed approach, but its reliance on gradient information made it susceptible to excessive segmentation. Deep learning-based methods such as Mask R-CNN can achieve high accuracy[8], but they require substantial computational resources and large annotated datasets, which restrict their applicability in resource-limited environments.

A key challenge in particle metrology is the development of robust, low-cost, and high-precision measurement systems capable of real-time operation[9]. Previous studies, including the work published in Heliyon[10], primarily addressed distance-map reconstruction to enhance watershed segmentation. However, this approach did not adequately incorporate gradient-based boundary constraints or real-time performance considerations.

Within the domain of dual-constrained or hybrid image segmentation, several studies have demonstrated the potential to handle complex, clustered objects. However, their application to agricultural particle metrology continues to face practical challenges. For instance, adaptive seed-marking and morphology-guided watershed variants have been successfully applied to blasted-rock and other granular imagery, yielding improved seed placement and reduced noise sensitivity[11]. Nonetheless, these approaches typically rely on multiple preprocessing stages and iterative refinements, which hinder their deployment in real-time scenarios using low-cost hardware.

Hybrid frameworks that combine edge- and region-based cues with post-segmentation merging, long investigated to mitigate over-segmentation, often increase computational overhead or introduce additional heuristic merging parameters[12]. In related biomedical and cell-clustering applications, recent methods that pair marker-controlled watershed with learned boundary predictors or lightweight CNN modules have achieved state-of-the-art separation for densely packed objects. However, these approaches rely on annotated datasets and GPU acceleration, which limit their deployment in resource-constrained agricultural environments[13].

More recently, distance-map reconstruction and improved distance-transform-based watershed variants have been proposed to enhance seed estimation and reduce fragmentation. Nonetheless, these methods often omit explicit gradient-based flooding control and rarely report real-time performance metrics relevant to online sorting applications.

At the technical level, existing segmentation algorithms exhibit limited effectiveness in identifying approaching particles, and dynamic detection accuracy remains insufficient[14,15]. The system's performance is heavily dependent on hardware capabilities, making it difficult to balance accuracy with cost[16,17]. At the application level, data-driven optimization of particle size thresholds is still underdeveloped, and effective integration between detection results and downstream processes such as seeding and sorting remains insufficient[18,19].

To address these challenges, we proposed a distance-gradient dual-constrained watershed algorithm, which integrated distance transform-based seed labeling with gradient-controlled flooding. This strategy effectively suppressed over-segmentation and enhances boundary preservation in densely packed particles. Furthermore, a low-cost, real-time machine vision system was developed to support quantitative extraction of multiple morphological parameters. Compared with conventional watershed segmentation, the proposed method improves segmentation accuracy by over 7% and reduces particle size measurement error by nearly 30%.

1 Material and method

1.1 Experimental material

In this experiment, three types of soybeans were used: Northeastern soybeans obtained from an online platform, and black and green soybeans purchased from a local farmers' market in Huaibei City, Anhui Province. The Northeastern variety features uniform grain shape, while the black and green soybeans reflect regional diversity, enhancing experimental generalizability.

The experimental setups include an industrial camera (HSK-200W), a Hikvon surface light source (MV-LBSS-120-120-W), a fixed lens bracket, and a host computer with Intel® Core™ i5-12400 CPU and NVIDIA RTX 4080 GPU (16 GB RAM), running Windows 10. Python 3.9 and OpenCV are used for image acquisition and processing (Fig.1). The HSK-200W camera provides 2-megapixel RGB imaging with stable performance and manual exposure/focus adjustment, suitable for fine particle analysis at low cost.

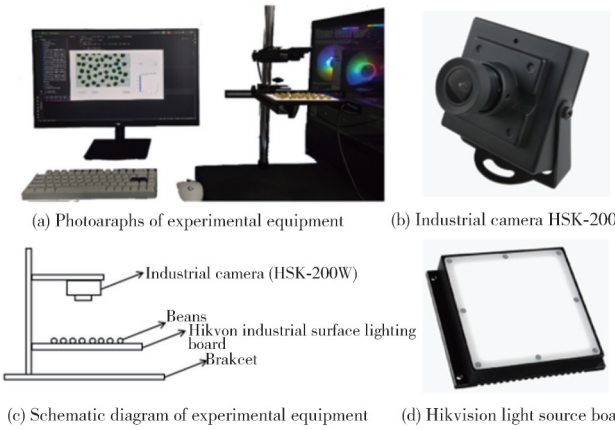

(a) Photoaraphs of experimental equipment (b) Industrial camera HSK-200W

(c) Schematic diagram of experimental equipment (d) Hikvision light source board

Fig. 1 Experimental equipment

1.2 System architecture

The proposed system integrates front-end acquisition and back-end analysis (Fig.2). Images are captured by the industrial camera and displayed in a PyQt-based GUI. Preprocessing includes grayscale conversion, denoising and enhancement. The algorithmic flow covers segmentation, watershed optimization, and feature extraction. The closed-loop design supports acquisition, visualization, measurement, and data export, ensuring scalability and applicability to agricultural seed analysis.

The core innovation lies in the synergistic integration of distance transform and gradient map constraints. The distance transform provides global, high-level shape information to generate robust internal markers, effectively controlling the number of segments and suppressing over-segmentation. Concurrently, the gradient map offers local, precise edge information to rigorously constrain the flooding process, ensuring that the resulting boundaries accurately align with the actual physical contours of the particles. This dual constraint mechanism fundamentally resolves the main drawbacks of the traditional watershed algorithm, namely its susceptibility to noise and the tendency to cause

excessive segmentation, as shown in Fig.3.

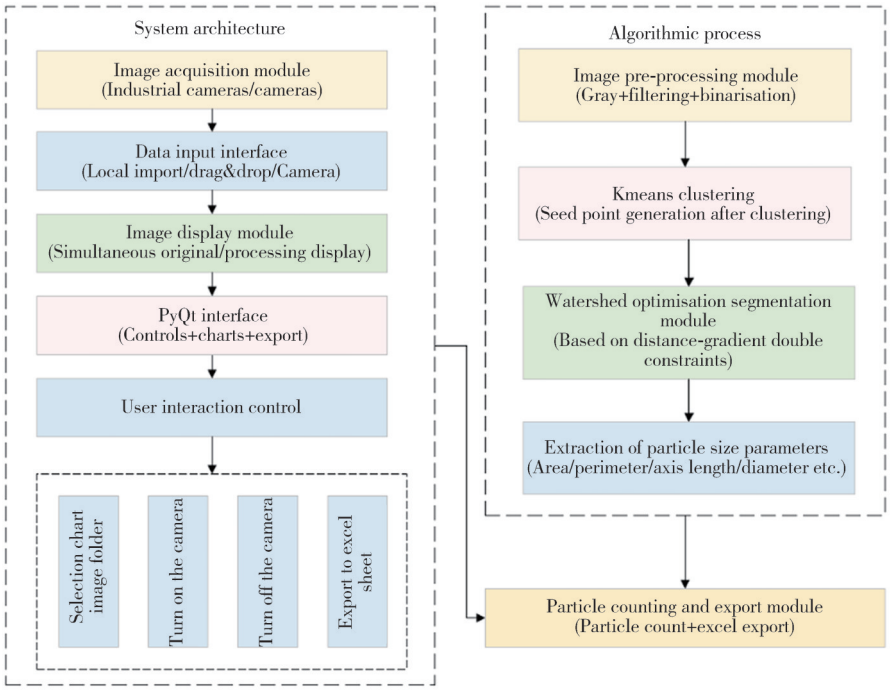

Fig. 2 Overall system architecture diagram

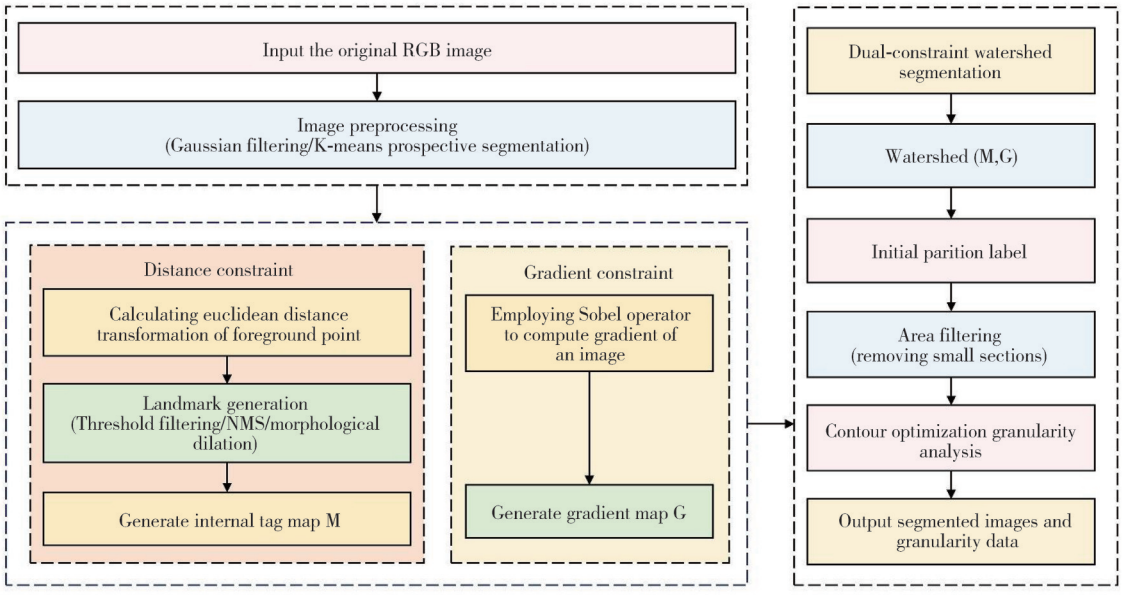

Fig. 3 Watershed optimisation algorithm with distance-gradient dual constraints

1.3 Image acquisition and pre-processing

Soybeans were evenly spread on the light plate to avoid overlap. The camera was mounted vertically with resolution fixed at 648 pixel×480 pixel. Illumination intensity, exposure, and contrast were adjusted for clarity, and images were transmitted to the host computer.

For noise reduction, Gaussian filtering was employed, as it provides smooth denoising while preserving edges, thereby ensuring robustness under uneven illumination. Following smoothing, the K-means clustering algorithm[20] was employed to segment the image into foreground and background.

In this context, let the image contain n pixels, where each pixel is represented by a feature vector $\boldsymbol{x}_i \in \boldsymbol{R}^d$, defined by its grayscale intensity or color components. The objective function that the K-means algorithm seeks to minimize is defined as[21]

$$J = \sum_{i=1}^{n}\sum_{j=1}^{k} r_{ij} \left\| \boldsymbol{x}_i - \boldsymbol{\mu}_j \right\|^2, \tag{1}$$

where $r_{ij} \in \{0,1\}$ indicates whether pixel $\boldsymbol{x}_i$ is assigned to the jth clustering centre $\boldsymbol{\mu}_j$, and k is the number of clustering centres (2 representing foreground and background,

respectively). K-means algorithm is shown in Fig.4.

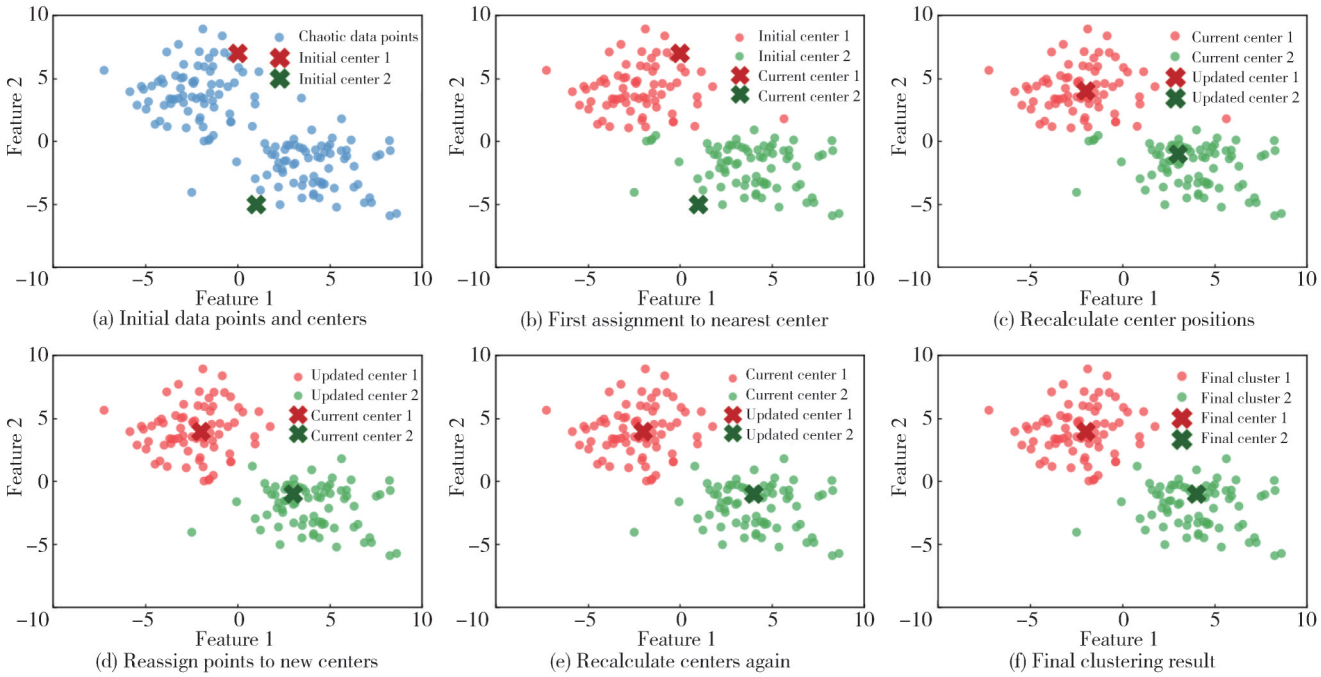

Fig. 4 Demonstration of K-means algorithm

1.4 Watershed optimisation algorithm based on distance-gradient double constraints

To clearly illustrate the implementation of the proposed distance-gradient dual-constrained watershed algorithm[22-24], Algorithm 1 outlines the complete computational procedure, from original image input to final granularity parameter output. The algorithm achieves high-precision segmentation of soybean grains through five key stages.

1) Image preprocessing employs Gaussian filtering and K-means clustering to generate a high-quality binary image.

2) Distance-constrained processing extracts accurate seed markers using Euclidean distance transformation and non-maximum suppression.

3) Gradient-constrained processing applies the Sobel operator to construct a boundary-sensitive gradient topography.

4) The dual-constrained watershed stage integrates distance and gradient information to achieve precise segmentation.

5) Post-processing extracts key granularity parameters through area filtering and ellipse fitting.

Algorithm 1 Distance-Gradient Dual Constraint Watershed Algorithm

Input: Raw RGB image I
Output: Segmentation label map L, Set of granularity parameters P
1: //**Phase 1: Image pre-processing**
2: $I_{gray} = RGB2Gray(I)$; //Convert to grayscale
3: $I_{smooth} = GaussianFilter(I_{gray}, \sigma = 1.5)$; //Gaussian filter denoising
4: $B_{binary} = KmeansSegmentation(I_{smooth}, k = 2)$; //K-Means binarization
5: //**Phase 2: Distance constraint processing**
6: $D = EuclideanDistanceTransform(B_{binary})$; //Compute Euclidean distance transform
7: $S = \varnothing$; //Initialize seed points set
8: **for** each piexl position (x, y) in B_{binary} **do**
9: **if** $(D(x,y) > \tau_d$ AND ((x, y) is local maximum of D)) **then**
10: $S = S \cup \{(x,y)\}$; //Filter seeds based on diatance threshold and NMS
11: **end if**
12: **end for**
13: $M = MorphologicalDilation(S, r = 3)$; //Generate connected labeled regions
14://**Phase 3: Gradient constraint processing**
15: $G = SobelGradient(I_{smooth})$; //Compute Sobel gradient magnitude
16: $G_{norm} = Normalize(G)$; //Normalize gradient map
17: //**Phase 4: Dual-constraint watershed segmentation**
18: $L = WatershedSegmentation(G_{norm}, M)$; //Watershed with gradient as topography and markers as sources
19: //**Phase 5: Post-processing and parameter extraction**
20: $L_{filtered} = AreaFiltering(L, A_{min} = 10)$; //Remove small regions by area filtering
21: $P = \varnothing$; //Initialize parameters set
22: **for** each connected region R_i in $L_{filtered}$ **do**
23: $contour_i = \text{FindContour}(R_i)$;
24: $A_i = CalculateArea(R_i)$;
25: $D_{eq} = \sqrt{\frac{4A_i}{\pi}} \times s$; //Calculate equivalent diameter, s is scale factor
26: $L_{major}, L_{minor} = EllipseFitting(contour_i)$; //Ellipse fitting for major/minor axes
27: $P = P \cup \{(D_{eq}, L_{major}, L_{minor}, A_i)\}$;
28: **end for**
29: **Return** $L_{filtered}, P$

The core innovation lies in the synergistic dual-constraint mechanism, which leverages the distance transform for accurate region counting and the gradient map for precise boundary localization.

1.4.1 Distance transformation and seed point generation

The Euclidean distance transform is applied to the

preprocessed binary image $B(x,y)$ to generate the distance map $D(x,y)$, which is mathematically defined as

$$D(x,y)=\min_{(u,v')\in\Omega_b}\sqrt{(x-u)^2-(y-v)^2}, \quad (2)$$

where Ω_b denotes the set of background pixel points, $B(x, y)=1$ is the foreground pixel point, and $D(x, y)$ is the Euclidean distance from that pixel point to the nearest background pixel. Marker points, which correspond to the centers of particles, are extracted by identifying the local maxima of $D(x, y)$ and applying morphological operations. These marker points serve as the initial seed locations (source points) for the subsequent watershed segmentation algorithm.

To extract valid watershed seed points, a distance threshold τ_d (set to $\tau_d>10$ pixels in this experiment) was first applied to filter out spurious edge peaks. Subsequently, an 8-neighborhood non-maximum suppression (NMS) [25] is performed to retain local maxima as candidate seeds, forming the set

$$S=\{s_i \mid D(s_i)\geqslant D(s_j),\forall j\in N_s(s_i)\}, \quad (3)$$

where $N_s(s_i)$ denotes the set of neighboring pixels around s_i. Morphological dilation with a radius $r=3$ pixels (used in this experiment) was then applied to S to generate a connected labeled domain $M(x,y)$, thereby preventing over-segmentation caused by discrete seed points, as shown in Fig.5.

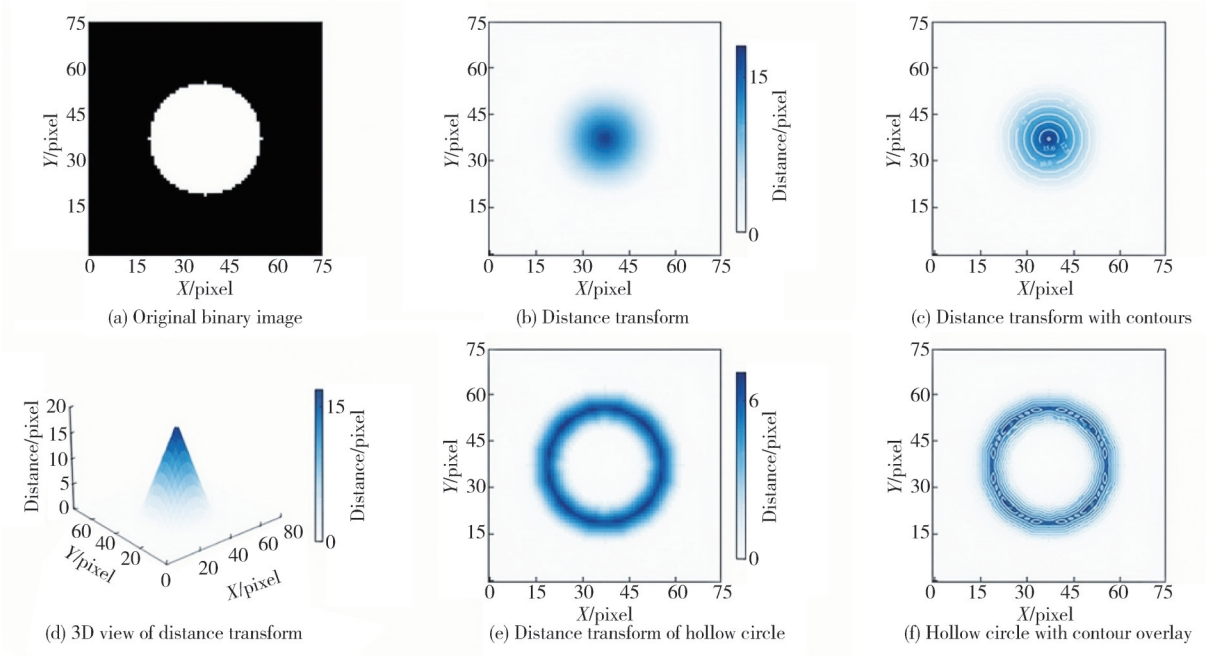

Fig. 5 Distance transformation

1.4.2 Watershed segmentation based on gradient map

In the classical watershed algorithm, an image gradient map is used to simulate topography and regulate the flooding process. In this study, the Sobel operator[26] was employed to compute the gradient image $G(x,y)$, which, together with the generated foreground marker map, was input into the watershed algorithm. The marker map serves as the "source points" to enforce controlled flooding initiation, thereby preventing over-segmentation caused by uncontrolled flooding.

The gradient magnitude $G(x, y)$ at each pixel is computed using the Sobel operator.

$$G(x,y)=\sqrt{\left(\frac{\partial I}{\partial x}\otimes \boldsymbol{K}_x\right)^2+\left(\frac{\partial I}{\partial y}\otimes \boldsymbol{K}_y\right)^2}, \quad (4)$$

where $\boldsymbol{K}_x=\begin{bmatrix}-1 & 0 & 1\\ -2 & 0 & 2\\ -1 & 0 & 1\end{bmatrix}$ and $\boldsymbol{K}_y=\boldsymbol{K}_x^{\mathrm{T}}$ represent the horizontal and vertical Sobel convolution kernels, respectively, and $I(x, y)$ denotes the original grayscale image.

The gradient field produces high-amplitude ridges at particle boundaries, providing topographical constraints for the watershed algorithm, as shown in Fig.6.

The resulting gradient map effectively highlights intensity transitions at object boundaries, which are used to constrain the flooding process during watershed segmentation.

Classical watershed segmentation can be formulated as an optimization problem that minimizes the total gradient along the region boundaries. The objective is to find a set of segmented regions $\{R_i\}$ that satisfies[27]

$$\min_{\{R_i\}} \sum_i \sum_{(x,y)\in\partial R_i} G(x,y), \tag{5}$$

where ∂R_i denotes the boundary of region R_i, and the goal is to minimize the cumulative gradient magnitude along these boundaries, thereby aligning segmentation lines closely with actual object contours.

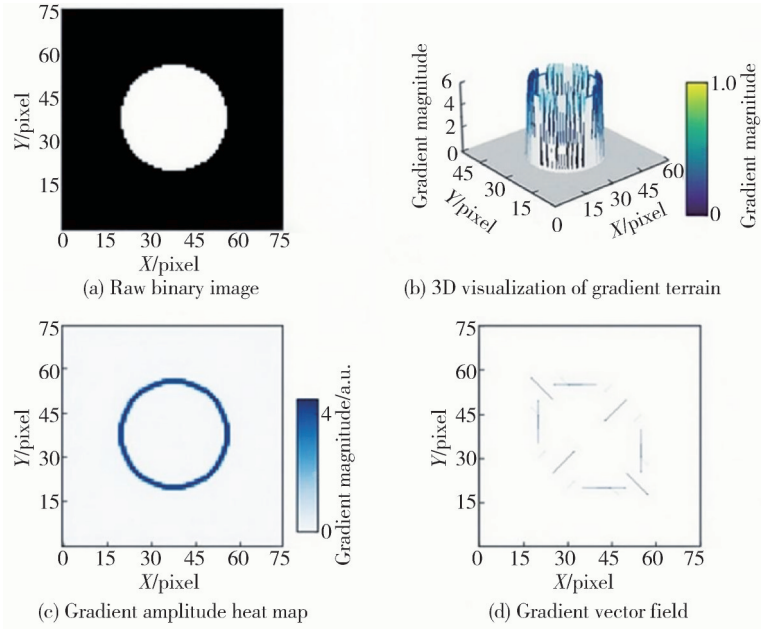

Fig. 6 Demonstration of gradient diagram

1.4.3 Joint distance-gradient constrained watershed

To integrate distance-based seed priors with gradient-based flooding regulation, we define a joint energy functional as

$$B_i = \sum_{(x,y)\in\partial R_i} G(x,y), \tag{6}$$

$$R_i = \sum_{(x,y)\in\partial R_i} \varphi\big(D(x,y), M(x,y)\big), \tag{7}$$

$$E(\{R_i\}) = \alpha_i B_i + \beta_i R_i, \tag{8}$$

where B_i enforces edge adherence via gradient constraints, R_i ensures consistency with distance-transform seeds, $\varphi\big(D(x,y), M(x,y)\big)$ is an indicator function that encourages flooding expansion outward from marker regions $M(x,y)$, α and β balance edge fidelity and seed guidance.

Minimization of Eqs. (6—8) corresponds to a marker-controlled watershed, where flooding is initiated at seed points from the distance transform and constrained by the gradient field. This dual-constraint strategy prevents over-segmentation and ensures particle boundaries closely match true contours.

1.4.4 Contour optimisation and particle size extraction

Post-processing removes spurious regions by enforcing a minimum area criterion.

$$A_i > A_{\min}, \quad i = 1, 2, \cdots, N, \tag{9}$$

where $A_i = 10$ pixels. For each valid contour, morphological features are extracted.

The equivalent diameter is calculated by

$$D_{eq} = \sqrt{\frac{4A}{\pi}} \cdot s. \tag{10}$$

The lengths of the major and minor axes[28] are derived from ellipse fitting as

$$L_{major} = \max(a,b)\cdot s, L_{minor} = \min(a,b)\cdot s. \tag{11}$$

The physical area in square millimeters is determined by

$$A_{mm^2} = A\cdot s^2, \tag{12}$$

where s is the pixel-to-physical scale factor (unit is mm/pixel).

2 Results

2.1 Performance evaluation of segmentation algorithm

We rigorously evaluated the efficacy of the proposed distance-gradient dual-constrained watershed algorithm, focusing primarily on its ability to accurately segment adjacent and contacting particles—one of the key challenges in granular image analysis.

To assess the practical performance of K-means clustering in segmenting bean particles, comparative experiments were conducted using both the Otsu thresholding method and the K-means clustering algorithm on the same batch of bean images. The evaluation metrics included segmentation accuracy (Accuracy), intersection over union (IoU), and edge preservation rate (EPR).

Representative results are shown in Table 1.

Table 1 Comparative analysis of segmentation effects

Method	Segmentation accuracy/%	IoU	Edge preservation retention/%
Otsu	85.40	0.73	78.60
K-means	93.80	0.84	87.30

Fig. 7 systematically presents the outputs of the proposed algorithm using three representative samples of different bean varieties. The first row shows the original RGB images, highlighting the initial adhesion among particles. The second row presents the K-means pre-segmentation results, which effectively separate the foreground beans from the background with high contrast and minimal noise, thus providing a clean binary image for subsequent processing.

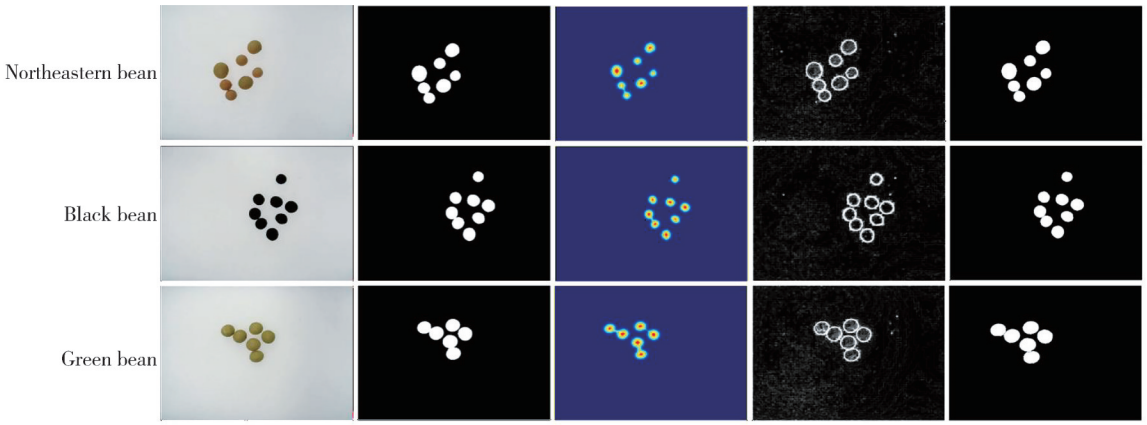

Fig. 7 Algorithm flow visualisation

The third and fourth rows display the core components of the dual-constraint mechanism: the distance transform map and the gradient map, respectively. The distance map identifies the centroid regions of each particle (bright areas), while the gradient map emphasizes the high-frequency boundary information between particles. The final row shows the segmentation results, where the boundaries of individual beans are accurately delineated and marked in distinct colors. Fig. 7 demonstrates that the proposed algorithm handles particles of varying sizes and colors effectively, and more importantly, resolves adhesion issues with high precision.

Fig. 8 provides a detailed close-up view of the segmentation process for a complex cluster of adhering particles.

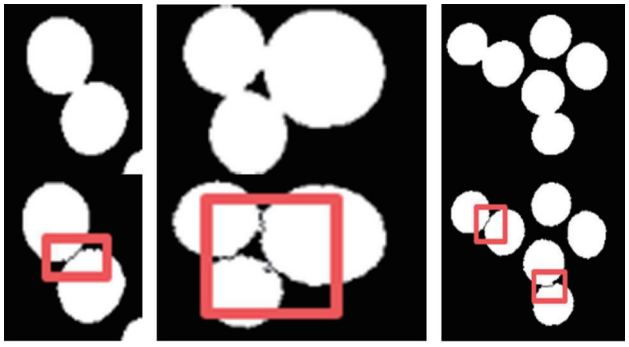

Fig. 8 Close-up view of segmentation of adherent particles

It compares the pre-segmentation image with the final result, clearly demonstrating how the algorithm successfully partitions contacting particles without under-segmentation (merging multiple particles into one) or over-segmentation (dividing one particle into multiple regions).

As shown in Table 2, the proposed algorithm reduced over-segmentation by 63.5% (from 8.5% to 3.1%) through morphological reconstruction and gradient correction. In contrast, the edge detection method exhibited boundary fragmentation with an 11.3% over-segmentation rate, while Otsu's thresholding produced a higher rate of 15.6%. For the measurement of particle size, the proposed method reduces the average error to 0.13 mm. Compared to the standard watershed algorithm, this improvement reaches 27.8%. This is due to the enhanced edge fidelity, which reduces the influence of segmentation artifacts on the size estimation.

Table 2 Segmentation effect of different algorithms

Algorithm	Segmentation accuracy/%	Oversplit ration/%	Average error/mm
Otsu threshold algorithm	82.30	15.60	0.27
Edge detection	85.70	11.30	0.21
Standard watershed algorithm	89.60	8.50	0.18
Algorithms in this study	96.80	3.10	0.13

2.2 Multi-species particle size characterisation

Tables 3—5 present the major dimensional parameters of the three primary cultivars, forming a morphological database that highlights the distinctions among varieties.

According to the Tables 3—5, the following conclusions

Table 3 Statistical characteristics of northeastern soybean particle size

Norm	Equivalent diameter/mm	Area/ mm^2	Perimeter/ mm	Longaxis/ mm	Shortaxis/ mm
Average	6.28	31.06	23.85	6.60	6.10
Standard	0.32	3.17	1.77	0.35	0.33
Min	5.71	25.60	20.25	5.94	5.49
Max	7.07	39.25	28.69	7.32	6.88

Table 4 Statistical characteristics of black soybean particle size

Norm	Equivalent diameter/mm	Area/ mm^2	Perimeter/ mm	Longaxis/ mm	Shortaxis/ mm
Average	6.81	36.55	23.08	7.15	6.56
Standard	0.38	4.04	1.46	0.49	0.41
Min	5.76	26.07	19.19	5.99	5.59
Max	7.49	44.09	26.10	8.22	7.22

Table 5 Statistical characteristics of green soybean particle size

Norm	Equivalent diameter/mm	Area/ mm^2	Perimeter/ mm	Longaxi/ mm	Shortaxis/ mm
Average	8.23	53.36	30.65	8.72	7.84
Standard	0.52	6.86	2.68	0.68	0.46
Min	7.36	42.53	25.90	7.65	6.89
Max	9.52	71.2	36.34	10.93	9.28

can be obtained. 1) The equivalent diameter exhibited significant varietal differences. Green soybean ((8.23±0.52) mm) > Black soybean ((6.81±0.38) mm) > Northeastern soybean ((6.28±0.32) mm) ($p<0.01$). 2) The aspect ratio (major axis/minor axis) follows the order: Green soybean (1.11), Black soybean (1.09), and Northeastern soybean (1.08), suggesting that more widely adapted varieties tend to exhibit greater morphological irregularity. 3) The coefficient of variation for particle area is highest in Green soybean (12.86%), followed by Black soybean (11.05%) and Northeastern soybean (10.21%).

These findings provide a quantitative basis for the design of sieve apertures in particle classification.

2.3 Metrological validation of measurement accuracy

To validate the metrological precision of the vision system, a manual verification was conducted using a precision vernier caliper. As shown in Table 6, the system's measurements of the major and minor axes for randomly selected seeds from each variety are in excellent agreement with the manual measurements.

Table 6 Comparison of bean seed measurements

Variety	Measurement number	Measuring short axis/mm	Measuring long axis/mm	Detection of short axis/mm	Detection of long axis /mm	Average error/%
Northeastern soybean	1	6.64	6.94	6.67	6.90	0.52
	2	6.50	6.78	6.33	6.68	2.05
	3	6.42	6.58	6.38	6.62	0.61
	Average	6.52	6.77	6.46	6.73	1.06
Black soybean	1	6.54	6.74	6.43	6.83	1.51
	2	7.34	7.60	7.15	7.75	2.42
	3	7.08	7.28	6.91	7.17	1.96
	Average	6.99	7.21	6.83	7.25	1.96
Green soybean	1	7.68	8.24	7.59	8.12	1.32
	2	7.80	8.44	7.68	8.31	1.54
	3	8.54	9.52	8.44	9.59	0.96
	Average	8.01	8.73	7.90	8.67	1.27

Equivalent diameter relationship is shown in Fig.9.

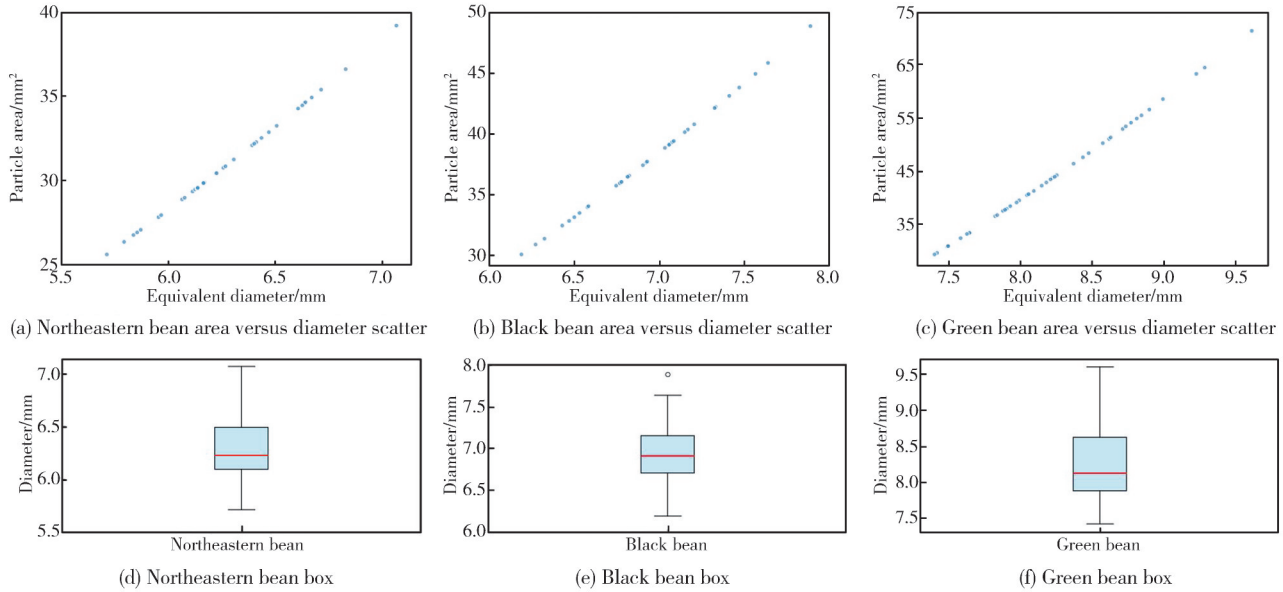

(a) Northeastern bean area versus diameter scatter (b) Black bean area versus diameter scatter (c) Green bean area versus diameter scatter

(d) Northeastern bean box (e) Black bean box (f) Green bean box

Fig. 9 Equivalent diameter relationship

The average absolute errors for the major and minor axes are exceptionally low: 0.04 mm/0.06 mm (0.59%/0.92%) for Northeastern soybeans, 0.04 mm/0.16 mm (0.55%/2.29%) for Black soybeans, and 0.06 mm/0.11 mm (0.69%/1.40%) for Green soybeans. The overall average relative error remained below 1.43%, which was well within the acceptable range for industrial-grade particle size analysis and confirmed the system's high reliability and measurement traceability. Correlation analysis between particle area and equivalent diameter (Fig.9a—c) yields a regression coefficient of R^2=0.962, demonstrating stable feature extraction.

Box plots (Fig. 9d—f) show compact distributions, particularly for Northeastern soybeans (IQR=0.41 mm), which is consistent with their uniform phenotype. Outlier rates remain below 3%, meeting the requirements specified in the GB/T 3543–1995 seed inspection standard.

The developed detection interface is tested for usability, as shown in Fig.10.

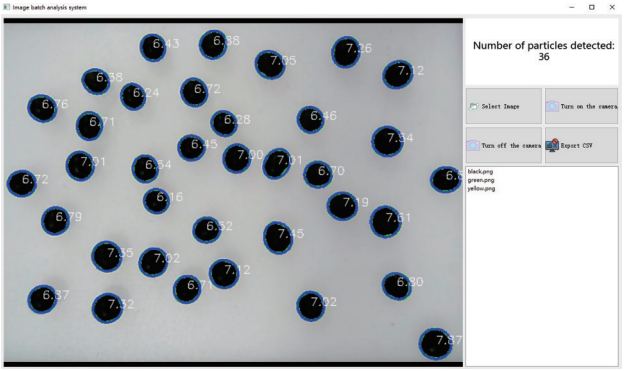

Fig. 10 System operation interface

3 Discussion

The proposed distance-gradient dual-constrained watershed algorithm was developed based on the general morphological and gradient characteristics of granular materials rather than species-specific features. As a result, the method demonstrates strong generalization capability and can be effectively applied to a wide range of soybean varieties as well as to other legume seeds with comparable adhesion and surface textures. In the present study, experiments on three soybean varieties—yellow, black, and green—consistently yielded high segmentation accuracy and stable particle size measurements across variations in surface brightness, color tone, and seed distribution.

From an application perspective, the algorithm has shown reliable performance under diverse imaging conditions, including multi-source illumination, daylight, artificial lighting, and desk-lamp environments. This robustness under varying noise and lighting disturbances underscores its practicality for real-world industrial scenarios, particularly for low-cost machine vision systems intended for small and medium-sized enterprises.

Although the current experiments primarily address typical separation scenarios, it is worth noting that heavily overlapping seed cases are uncommon in actual processing and metrology workflows due to the use of mechanical dispersion devices. Nevertheless, investigating algorithmic adaptations for more complex overlapping or cluttered scenes remains an important direction for future research, which could further enhance the system's applicability in dense-packing or mixed-material agricultural datasets.

4 Conclusions

The proposed distance-gradient dual-constrained watershed algorithm achieved a segmentation accuracy of 96.8% and a mean particle diameter error of only 0.13 mm, marking a 27.8% improvement over the traditional watershed method. This enhancement is attributed to two key components: (1) a distance-based marker strategy that reduced over-segmentation to 3.1% through morphological dilation, and (2) a gradient-constrained flooding mechanism that improved contour alignment (IoU: 0.84). These improvements mitigated edge fragmentation and excessive seed generation, outperforming previous methods by 15.6% and 8.5%. When combined with K-means pre-segmentation, the system exhibited strong illumination adaptability (edge retention: 87.3% vs. Otsu's 78.6%), enabling real-time performance using low-cost hardware. This makes the system practical for small and medium-sized enterprises.

However, challenges remain in segmenting heavily overlapping particles and maintaining robustness under dust interference. Future work will focus on integrating multispectral imaging and establishing a comprehensive particle size–quality database to support precision sorting and sowing in agricultural applications. In addition, efforts will be directed toward improving the segmentation accuracy of adherent or overlapping particles, which remains a key challenge in enhancing the robustness and reliability of the system under complex field conditions.

Acknowledgement

This work was supported by National Natural Science Foundation of China (No. 62006092), University Synergy Innovation Program of Anhui Province (No. GXXT-2023-108), and Excellent Youth Project of Natural Science

Research in Anhui Province (No. 2023AH030081).

Declaration of conflicting interests

The authors have no conflict of interests related to this publication

References

[1] ALVES A K S, ARAÚJO M S, CHAVES S F S, et al. High throughput phenotyping in soybean breeding using RGB image vegetation indices based on drone. Scientific Reports, 2024, 14: 32055.

[2] WANG J L, HE J L, HAN Y, et al. An Adaptive Thresholding algorithm of field leaf image. Computers and Electronics in Agriculture, 2013, 96: 23-39.

[3] WANG Q F, CHENG M, XIAO X P, et al. An image segmentation method based on deep learning for damage assessment of the invasive weed Solanum rostratum Dunal. Computers and Electronics in Agriculture, 2021, 188: 106320.

[4] ZHU L L, SPACHOS P, PENSINI E, et al. Deep learning and machine vision for food processing: a survey. Current Research in Food Science, 2021, 4: 233-249.

[5] JIA H M, SU Y Y, RAO H H, et al. Improved artificial rabbits algorithm for global optimization and multi-level thresholding color image segmentation. Artificial Intelligence Review, 2024, 58(2): 55.

[6] TAN C, JIANG Y, LI Q, et al. Computed tomography point cloud segmentation of complex industrial components via structural features and region growing algorithm. Measurement, 2026, 257(PB): 118742-118742.

[7] WANG X C, WU X L, DING G H, et al. Analysis of grain yield differences among soybean cultivars under maize-soybean intercropping. Agronomy, 2020, 10(1): 110.

[8] KUMAR M, CHANDEL N S, SINGH D, et al. Soybean disease detection and segmentation based on mask-RCNN algorithm. Journal of Experimental Agriculture International, 2023, 45(5): 63-72.

[9] WU Y Y, LI Q. The algorithm of watershed color image segmentation based on morphological gradient. Sensors, 2022, 22(21): 8202.

[10] LIU H Q, ZHANG W J, WANG F S, et al. Application of an improved watershed algorithm based on distance map reconstruction in bean image segmentation. Heliyon, 2023, 9(4): e15097.

[11] GUO Q P, WANG Y C, YANG S J, et al. A method of blasted rock image segmentation based on improved watershed algorithm. Scientific Reports, 2022, 12: 7143.

[12] WOLF S, SCHOTT L, KÖTHE U, et al. Learned watershed: end-to-end learning of seeded segmentation//2017 IEEE International Conference on Computer Vision, October 22-29, 2017, Venice, Italy. New York: IEEE, 2017: 2030-2038.

[13] LUX F, MATULA P. Cell segmentation by combining marker-controlled watershed and deep learning. arXiv preprint arXiv:2004.01607, 2020.

[14] LIU S X, CHEN D J, PLUMIER B, et al. Impact of particle size fractions on composition, antioxidant activities, and functional properties of soybean hulls. Journal of Food Measurement and Characterization, 2021, 15(2): 1547-1562.

[15] AGUILAR-GONZÁLEZ A, MEDINA SANTIAGO A, OROZCO TORRES J A, et al. TurboPixels: a superpixel segmentation algorithm suitable for real-time embedded applications. Applied Sciences, 2024, 14(24): 11912.

[16] ZHANG Y W, LI W, LIN Y H, et al. Construction of a high-density genetic map and mapping of QTLs for soybean (Glycine max) agronomic and seed quality traits by specific length amplified fragment sequencing. BMC Genomics, 2018, 19(1): 641.

[17] LIU Y, ZHANG Y W, WANG Y. Application of deep learning-based image processing in emotion recognition and psychological therapy. Traitement Du Signal, 2024, 41(6): 2923-2933.

[18] XU J J, LU Y Z, DENG B Y. OpenWeedGUI: an open-source graphical tool for weed imaging and YOLO-based weed detection. Electronics, 2024, 13(9): 1699.

[19] SINHA S, NETHI A, JETTA M. Multiplicative Gaussian noise removal using partial differential equations and activation functions: a robust and stable approach//7th International Conference on Algorithms, Computing and Systems, Larissa Greece. New York: ACM, 2023: 161-170.

[20] SILVA-BLANCAS V H, JIMÉNEZ-HERNÁNDEZ H, HERRERA-NAVARRO A M, et al. A clustering and PL/SQL-based method for assessing MLP-kmeans modeling. Computers, 2024, 13(6): 149.

[21] CHINNAKANNAN N, NALLAMUTHU P. Using KMeans clustering to evaluate and alert for deviations of linac photon beam parameters. Asian Pacific Journal of Cancer Prevention, 2024, 25(1): 305-315.

[22] MOSTAFA R R, HOUSSEIN E H, HUSSIEN A G, et al. An enhanced chameleon swarm algorithm for global optimization and multi-level thresholding medical image segmentation. Neural Computing and Applications, 2024, 36(15): 8775-8823.

[23] OLLE OLLE D G, ZOOBO BISSE J, ABESSOLO ALO'O G. Application and comparison of K-means and PCA based segmentation models for Alzheimer disease detection using MRI. Discover Artificial Intelligence, 2024, 4(1): 11.

[24] SHYAMALA N, MAHABOOBBASHA S. Watershed algorithm with YOLO: A hybrid approach for brain tumor identification and segmentation. Journal of Physics: Conference Series, 2025, 3038(1): 012009.

[25] ZHAO Z, LI B, KANG X Q, et al. Hybrid image segmentation method based on anisotropic Gaussian kernels and adjacent graph region merging. The Review of Scientific Instruments, 2020, 91(1): 015104.

[26] BALASUBARAMANIAN S, SHAN M A. Restricted Boltzmann machine with Sobel filter dense adversarial noise secured layer framework for flower species recognition. Scientific Reports, 2025, 15(1): 1-30.

[27] FURAT O, KIRSTEIN T, LEIßNER T, et al. Multidimensional characterization of particle morphology and mineralogical composition using CT data and R-vine copulas. Minerals Engineering, 2024, 206: 108520.

[28] SINKHONDE D. Major and minor elliptical axes and bounding rectangle dimensions in clay brick powder particles from changing milling conditions. Cleaner Waste Systems, 2023, 6: 100123.

一种用于豆类颗粒分割与尺寸测量的双约束分水岭算法

庄立城, 葛博昂, 胡 俊, 宋毅恒, 刘 升*

淮北师范大学 人工智能学院, 安徽 淮北, 235000

摘 要： 精确测量豆粒大小对于农产品加工中的自动分级和质量控制至关重要，但现有的图像分割方法往往存在效率低、过度分割和计算成本高等问题。本文提出了一种距离梯度双约束分水岭算法，用于精确分割和测量豆粒。该方法将基于距离变换的种子提取与梯度约束泛洪相结合，有效抑制了噪声引起的区域破碎，提高了附着颗粒的分离效果。为了评估该方法的性能，我们利用工业相机和图像处理流水线搭建了一个实验平台。与传统的分水岭算法相比，所提出的方法将分割精度提高了7.2％，并将平均粒度误差降低了27.8％(0.13 mm，相对误差2.4％)。在三个大豆品种上的验证证实了该方法的通用性。结果表明，所提出的算法为农业粒度分析提供了一种高效、准确的技术，有望被集成到实用的低成本检测系统中。

关键词： 距离-梯度双约束分水岭算法；机器视觉检测系统；粒度分拣；精准农业；计量学

引用格式： ZHUANG Licheng, GE Boang, HU Jun, et al. A dual-constrained watershed algorithm for bean particle segmentation and sizing. Journal of Measurement Science and Instrumentation, 2025, 16(4): 526-536. DOI: 10.62756/jmsi. 1674-8042.2025051